Residual Stress Distributions in Arc, Laser and Electron-Beam Welds in 30 mm Thick SA508 Steel

DOI:
10.1016/j.ijpvp.2018.03.004

Document Version
Accepted author manuscript

Residual Stress Distributions in Arc, Laser and Electron-Beam Welds in 30 mm Thick SA508 Steel: A Cross-Process Comparison

J. Balakrishnan*[a,b], A. N. Vasileiou[a], J. A. Francis[a], M. C. Smith[a], M. J. Roy[a], M. D. Callaghan[a] and N. M. Irvine[c]

[a]School of Mechanical, Aerospace and Civil Engineering, The University of Manchester, Manchester M13 9PL, U. K.
[b]Nuclear AMRC, University of Sheffield, Rotherham S60 5WG, U.K.
[c]Dalton Nuclear Institute, The University of Manchester, Manchester M13 9PL, U.K.

***Corresponding author:** Nuclear AMRC, University of Sheffield, Advanced Manufacturing Park, Brunel Way, Rotherham S60 5WG, U.K. **E-mail:** jey.balakrishnan@namrc.co.uk

Abstract: Safety-critical pressure vessels in pressurised water reactor (PWRs), such as the reactor pressure vessel and the steam generators, have been fabricated using arc welding processes for several decades. However, recent interest in nuclear new-build programmes has stimulated interest in reassessing the technologies that are available for the welding of these components. For example, considerable effort has been directed at the development of reduced-pressure electron beam (RPEB) welding, owing to the substantial productivity gains it would offer, while developmental work has also been carried out on multipass narrow-gap laser welding (NGLW). In this work we assess the effects that two current technologies, and two candidate technologies for future build programmes, are likely to have on the generation of residual stresses within critical nuclear components. Single-sided welds were manufactured in 30 mm thick plates of SA508 steel, using four welding processes: gas-tungsten arc welding (GTAW), submerged-arc welding (SAW), multipass NGLW and RPEB welding. The residual stress distributions for each type of weld have been measured both in the as-welded condition and after post-weld heat treatment, using neutron diffraction and the contour method. The results are compared and discussed.

Keywords: conduction mode welding, ductile-to-brittle transition, pressuriser, structural integrity, weld integrity, weld toughness.

1 Introduction and background

Arc welding processes have been a mainstay in the manufacture of primary components within pressurised water reactors (PWRs), such as the reactor pressure vessel (RPV) and the steam generators, for several decades. Indeed, fabrication standards such as those that are overseen by professional associations such as the American Society for Mechanical Engineers (ASME) currently prohibit the application of alternative welding technologies to these safety-critical components. This circumstance has lingered since a significant slowdown that was seen, particularly in the U.S.A., in the initiation of nuclear new-build projects following the Three Mile Island accident in 1979 and the Chernobyl disaster in 1986. However, in the past decade, the prospect of an increase in the construction of new PWRs has prompted some in the nuclear sector to re-examine the options for the welding of these large ferritic pressure vessels.

One process that has been the subject of significant interest in recent years is reduced-pressure electron beam (RPEB) welding [1, 2]. The prospect of completing welds that exceed 100 mm in thickness with a single weld pass is clearly attractive from an economic standpoint. Furthermore, by welding under a reduced pressure, as opposed to under a high vacuum, it becomes possible to employ local sealing systems, rather than having to place an extremely large pressure vessel inside a vacuum chamber [1]. However, if a strong case is to be made for the adoption of a process such as RPEB welding, potential economic benefits must be accompanied by reassurances that the integrity of these safety-critical components will not be compromised. To this end, one of the factors that must be considered is the development of residual stresses.

Tensile residual stresses are known to have detrimental effects on the integrity of pressure vessels in light water reactors [3], as they can increase the driving force for crack propagation [4], and they can also contribute to degradation through mechanisms such as stress-corrosion cracking [5]. Fusion welding processes are also known to generate substantial tensile residual stresses [6], owing to the highly localised manner in which heat is applied, and the associated steep temperature gradients that are imposed on the materials being joined. Indeed, the significance of welding residual stresses to nuclear safety has been recognised in the R6 Defect Assessment Procedure [7], which requires an account of residual stresses in the vicinity of welds in primary nuclear components. Residual stresses

are also likely to be of concern to other industries that deploy pressure retaining vessels and piping such as, for example, in the petrochemical sector, notwithstanding the fact that such applications appear to have received less attention.

In the case of ferritic steels, the development of welding residual stresses is complicated by the solid-state phase transformations that take place during welding thermal cycles [8] and, while ferritic steel welds are subject to a post-weld heat treatment (PWHT) operation, this does not eliminate residual stresses altogether [9]. The complicated nature of the development of residual stresses in multipass ferritic steel welds has led to a variety of studies being carried out, ranging from those that investigate a single weld pass [10, 11], to others dealing with multiple weld passes [12, 13]. However, to date, studies on the development of residual stresses in nuclear steels have generally focused on a specific welding technology, and it has been difficult to directly compare the extent to which alternative welding processes will influence the development of stress.

Within the NNUMAN research programme [14], a decision was taken to manufacture welds in nuclear pedigree SA508 Grade 3 Class 1 steel, using both current arc-based technologies and candidate technologies for future nuclear new build programmes. The objective was to assess the implications associated with a particular choice of welding process for the through-life integrity of nuclear components, and one of the parameters that would be used in undertaking such an assessment was to be the development of residual stresses. The authors formed the view that, to carry out such an assessment, it would be important to manufacture welds at a thickness that is representative for nuclear pressure vessels.

After assessing options for the procurement of material of a suitable pedigree, the target weld thickness was chosen to be 130 mm. However, it soon became evident that a significant amount of development work would be required on the journey to manufacturing welds at this thickness. Consequently it was also decided that, as a first step, weld test pieces should be manufactured with the same welding processes at a smaller thickness. To this end, a thickness of 30 mm was selected, as this would provide test pieces that would capture many aspects of multipass welding, yet they would also be amenable to residual stress measurements using non-destructive techniques such as neutron diffraction.

This article commences by describing the manufacture of 30 mm thick welds in SA508 Grade 3 Class 1 steel using the following techniques:

- Narrow-gap submerged arc welding (NG-SAW);

- Narrow-gap gas-tungsten arc welding (NG-GTAW);
- Multipass narrow-gap laser welding (NGLW); and
- Reduced pressure electron beam (RPEB) welding.

The measurement of residual stresses is subsequently described, on test pieces in both the as-welded (AW) and PWHT condition, using neutron diffraction and the contour method. The results are then presented and discussed. It is hoped that this work will serve to provide insights to the development of residual stresses with each of these welding processes, while also providing valuable validation cases for the development of weld models.

2 Manufacture of Weld Test Pieces

2.1 Materials

Four weld test pieces were made using each of the welding processes employed in this study, making 16 in total. In all cases, the base material was SA508 Grade 3 Class 1 steel, with the chemical composition as given in Table 1. This steel was purchased from Sheffield Forgemasters International Ltd. in the form of a prolongation ring forging together with thinner segments of material extracted from the dome that was contiguous with the prolongation ring. The forged SA508 material had already been subjected to a quality heat treatment at the time it was supplied to The University of Manchester. In this condition, the yield stress of this steel has been found to be approximately 450 MPa and the ultimate tensile strength (UTS) was in the range between 560 and 600 MPa [12].

All of the NG-SAW, NG-GTAW and NGLW test pieces were welded at The University of Manchester, while those for the RPEB process were welded at TWI Ltd. For the NG-GTAW and NGLW test pieces, a filler wire with a diameter of 1.2 mm was used. This filler wire was supplied without a copper coating, since the presence of copper is known to increase the susceptibility of nuclear steels to irradiation embrittlement [15]. For the NG-SAW test pieces, a copper-coated filler wire with a diameter of 2.4 mm was used. The decision to use a copper-coated wire in the case of the NG-SAW test pieces was justified on the basis of cost, and also on the grounds that the larger wire diameter mitigated the presence of a copper coating to the point where the copper concentration in the NG-SAW filler wire was lower than it was for the NG-GTAW filler wire (which did not have a copper coating). The RPEB welds were unaffected by the choice of filler wire since they were autogenous. The

chemical compositions for the filler wires that that were used in each type of weld are also given in Table 1.

Table 1: Chemical compositions of SA508 Gr. 3 Cl. 1 steel and filler materials (wt.-%)

Materials/Elements	C	Si	Mn	Cr	Co	Ni	Mo	S	P	Cu	Fe
SA508Gr.3Cl.1	0.16	0.27	1.43	0.23	0.004	0.77	0.52	0.002	0.005	0.04	Bal.
SDX S3Si-EH12K (NG-SAW)	0.08	0.37	1.48	0.012	-	0.037	0.003	0.005	0.008	0.054	Bal.
ENi5 (S31Ni1/4Mo) (NG-GTAW/CWL)	0.10	0.20	1.47	0.03	-	0.88	0.25	0.005	0.006	0.075	Bal.

2.2 Design of Test Pieces

In all cases the weld test pieces had dimensions of approximately 415 mm × 145 mm × 30 mm (Fig. 1). The design of the 30 mm thick specimens changed slightly depending on the welding process that was to be applied. While an important function of these specimens was to serve as a milestone in the development of welding procedures for 130 mm thick joints, the specimens were also designed in a way that made them suitable benchmarks for the validation of the finite-element (FE) modeling methodologies, which were being employed within the NNUMAN research programme for the prediction of residual stresses.

One of the key difficulties in the modeling of residual stress development in welds relates to the quantification of the restraint that is applied to the specimen. Welding laboratories often feel tempted to use what is often described as “rigid clamping” in order to prevent excessive distortion during welding operations. However, “rigid restraint” is often very difficult to quantify precisely, as in practice it is not perfectly rigid, and it does not lead to zero deflection at the restrained locations. While this may not be troublesome to experimentalists, it does create difficulties in the prediction of residual stresses. For this reason, an unconventional specimen geometry was employed for the NG-SAW, NG-GTAW and NGLW samples. These welding techniques all involved the use of multiple weld passes from one side of the test piece, thereby contributing to a strong tendency for “butterfly” distortion. This type of distortion involves the apparent rotation, about the weld centerline, of the plate segments on either side of the weld centreline. The weld centreline in Figure 1 is parallel to the z-axis, and butterfly distortion would lead to the plate surfaces on either side of the weld centerline moving in what is denoted as the positive y-direction.

For the multipass specimens, the design of the test piece was such that a ligament of material was left intact at either end of the weld (See Fig. 1). This meant that the specimens had an inbuilt degree of self-restraint, which would resist butterfly distortion. As such, the specimens did not require any significant restraint, as they needed only to be prevented from translating on the support plate during welding operations. With the application of very little restraint, one can have greater confidence that the restraint boundary conditions are not having a significant influence on the residual stresses that are predicted in numerical analyses. Furthermore, the inbuilt restraint associated with the specimen design can easily be captured within a numerical model by recreating the specimen geometry accurately.

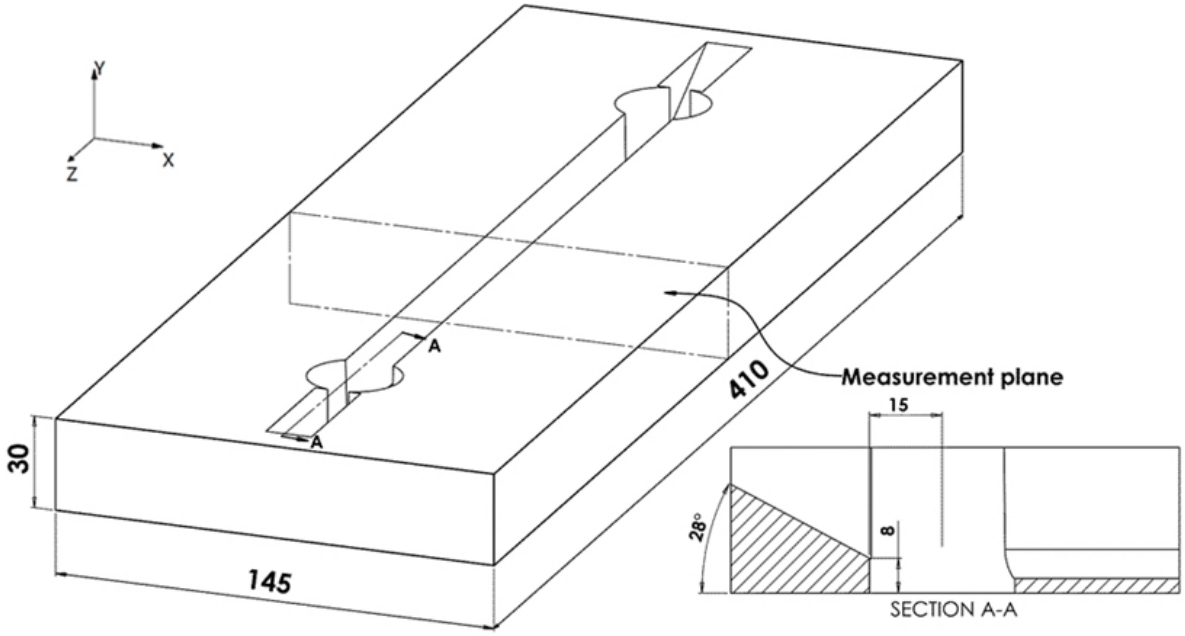

Figure 1: Schematic representation of overall specimen geometry for welding experiments at a thickness of 30 mm. Although not shown here, the weld groove geometry varied according to the welding process.

The only weld test pieces that deviated from the configuration shown in Figure 1 were the RPEB welds, which were manufactured at TWI Ltd. The RPEB welds were single pass “keyhole” welds. The manufacture of a single pass weld with a deep and narrow fusion zone geometry, in which the width of the fusion zone remains almost constant throughout the thickness, does not lead to significant levels of butterfly distortion. As such, it was possible to use the full length of the machined plates for the purpose of welding.

It can be seen in Fig. 1 that, in each of the multipass weld test pieces, holes were machined in the plates in such a way that they effectively shortened the weld groove, and in doing so created the ligaments of material at both ends of the plate. The holes were incorporated to simulate the end of a plate, in the hope that the final test pieces would be representative of groove welds, as opposed to slot welds. The distinction between these categories is that a groove weld traverses the entire length of the plate, whereas a slot weld involves the deposition of metal into a slot that traverses only some portion of the plate length. Slot welds, therefore, could be expected to have residual stress distributions that differ from those of groove welds. The incorporation of the holes in the multipass weld specimens resulted in the nominal weld length being reduced to 240 mm. Finally, it can be seen in Fig. 1 that the ligaments of material at either end of the weld were not uniform in thickness. This ligament geometry was chosen as a compromise between leaving as much material intact as possible (i.e. to provide restraint) while also providing enough room for the entry and withdrawal of the welding torch during the run-in and run-out procedures.

2.3 Welding Parameters and Bead Stacking Pattern

The weld groove geometry and the weld bead stacking pattern are shown in Figure 2 for each welding process. The groove geometries alone appear on the left hand side of the figure, while bead stacking patterns are shown on the right. The narrow-gap laser welding technique (NGLW) utilised a much narrower weld groove than those for NG-SAW and NG-GTAW. The locations at which thermocouples were attached to each test piece also appear in the figure. However, the recorded thermal cycles were needed primarily for the validation of numerical models in future work and, as such, they will not be presented in this article. A summary of the basic welding parameters that were employed in the manufacture of each type of weld test piece is given in Table 2.

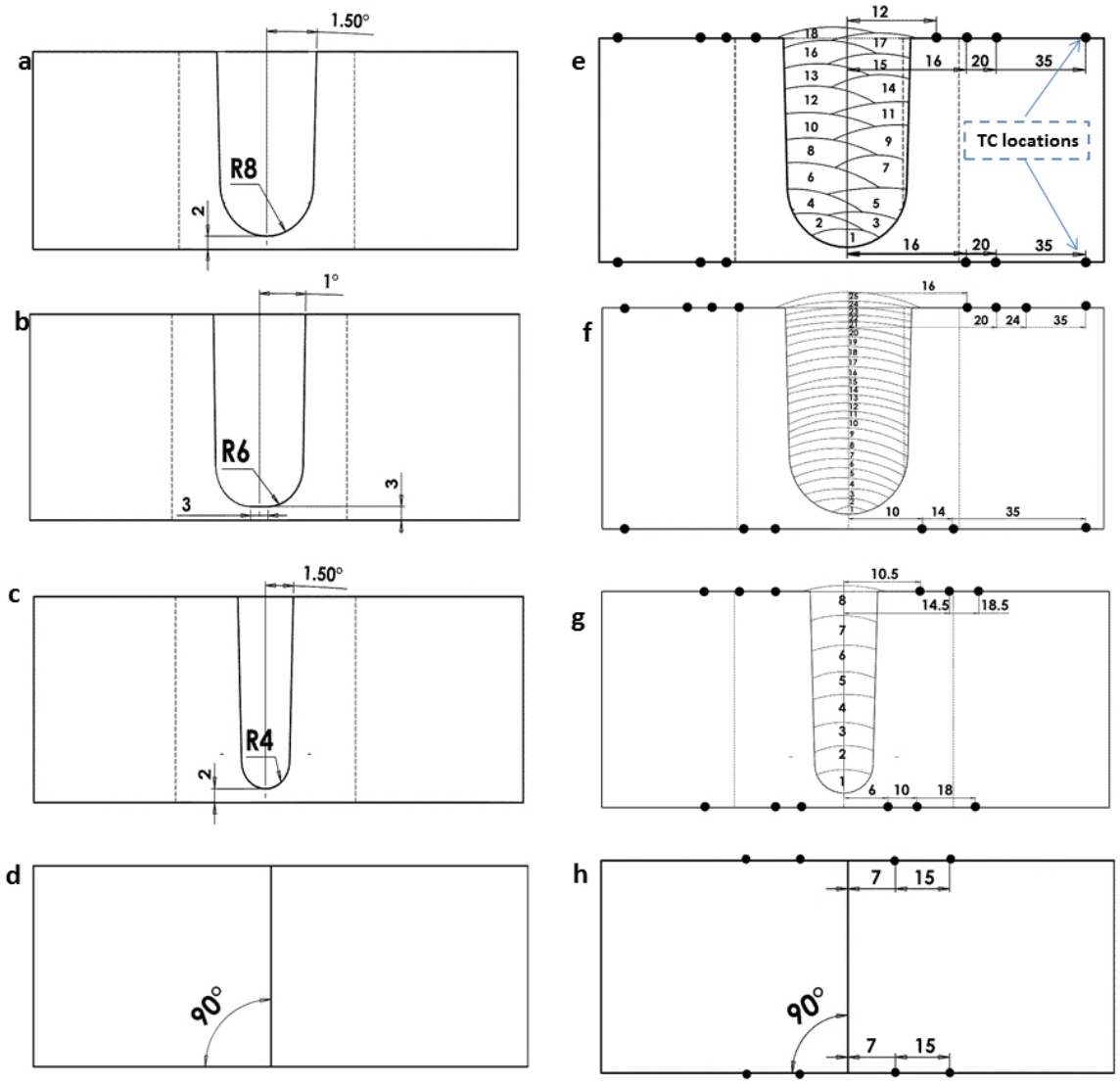

Figure 2: Details of the weld groove geometry and bead stacking pattern for (a) NG-SAW, (b) NG-GTAW, (c) NGLW and (d) RPEB welding. The locations at which thermocouples were attached are also shown for each specimen type.

For the welding of the NG-SAW, NG-GTAW and NGLW test pieces, argon was used as the shielding gas, while the RPEB specimen was welded in a vacuum at a pressure of 3×10^{-2} mbar. In all cases, a preheat/interpass temperature of between 100 and 165°C was maintained. After welding, two of the four welds that were made with each welding process were subjected to a PWHT operation, while the other two were preserved in the AW condition. The PWHT procedure did not place restrictions on the heating and cooling rates below 300°C, but the heating and cooling rates were restricted to a maximum of 20°C per hour between 300 and 607 °C, and the soak took place at a temperature of 607 +/- 13 °C for a duration of 2 hours.

Table 2: Typical Process Parameters Used in the Manufacture of Weld Test Pieces

	NG-SAW	NG-GTAW	NGLW	RPEB
Voltage (V)	27	11	7 kW	150000
Current (A)	225/350	275/325		0.09
Welding Speed (mm/min)	450/325	75	240	200
Pulsing Frequency (Hz)	N/A	1	N/A	N/A
Beam diameter (mm)	N/A	N/A	6	2
Wire diameter (mm)	2.4	1.2	1.2	N/A
Wire Feed Speed (m/min)	-	0.8 – 1.0	5	N/A
Welding position	1G	1G	1G	2G
Heat Input (kJ/mm)	0.8-1.7	2.4-2.9	1.8	4.1

The authors did consider selecting welding parameters for each technique that would have led to a reduction in the range in weld heat input that was investigated in this study (see Table 2). However, there were two factors that contributed to a decision in favour of the parameters that were selected. The first is that it would not have been viable to manufacture test pieces with each of the welding processes, while using the same weld heat input in each case, without deviating significantly from the parameters that would typically be employed with each process in practice. Thus, such a choice would have raised questions relating to the extent to which this study is representative of welding practice. The second consideration was that, while a systematic comparison of these welding processes has not been carried out previously, it has been established that the extent of the residual stress distribution in arc welds [10, 16] and in electron beam welds [17] correlates with the extent of the metallurgical zones within the weldment. It can therefore been argued [10] that the influence of the weld heat input will be evident through its influence on the extent of the metallurgical zones in a welded joint.

2.4 Nondestructive Evaluation

All welds were radiographed, and all welds were found to be free of significant defects, according to the acceptance criteria in ASME IX: 2013.

The distortion associated with each of the welded joints was also captured using a Creaform EXAscan laser scanning system (Handyscan 700). This is a hand-held system that enables surface profiles and distortion to be measured in three dimensions, with a maximum resolution of 0.05 mm and a maximum accuracy of 0.03 mm. The data that was obtained was used to obtain an estimate for the butterfly distortion angle, where an angle of zero corresponds to the welded test piece remaining perfectly flat after welding (i.e. no butterfly distortion).

2.5 Metallography and Hardness Measurements

For each weld type, one specimen in the AW condition and one in the PWHT condition were allocated for destructive residual stress measurements using the contour method, as well as for the extraction of macrograph slices. The macrograph sections were polished to a 1 μm finish before they were etched using a solution of 5 ml nitric acid and 95 ml ethanol. Microstructural examination was carried out using a KEYENCE VHX-500F optical microscope. The variation in microhardness across the joints was measured using a Vickers microhardness machine (DurascanTM) with a load of 0.5 kg and a dwell period of 20 s. The measurement array spanned the fusion zone and heat-affected zone (HAZ) in each welded specimen, as well as a few millimetres of the adjacent parent material, until the hardness values stabilized. The density of measurements changed for each welding process, depending on the microstructure gradients that were expected. Typically, a rectangular measurement array was used, with measurement intervals varying between 0.25 and 1 mm.

2.6 Neutron Diffraction Measurements

The residual stresses in the NG-SAW, NGLW and the RPEB test pieces in the AW condition were measured using the Engin-X beam line at the ISIS Neutron and Muon Source in the U.K. The residual stresses in the NG-GTAW test piece in the AW condition, and in the NG-SAW and RPEB welds in the PWHT condition, were measured at the SALSA beam line at the Intitut Laue-Langevin (ILL) in Grenoble, France. Finally, the residual stresses in the NG-GTAW and NGLW specimens in the PWHT condition were measured at the Kowari beamline at the Australian Nuclear Science and Technology Organisation (ANSTO) at Lucas Heights, N.S.W., Australia.

The significance of the measurement location is associated with the method in which neutrons are generated. ISIS is a spallation source, which employs the time-of-flight technique to measure strains within crystalline materials. This results in the simultaneous measurement of strains on different crystallographic planes within the material, so that the resulting measurements are less sensitive to errors associated with texture [18]. The raw time-of-flight data are subjected to a Pawley-type [19] spectrum refinement based on the General Structure Analysis System (GSAS) software [20]. This procedure results in an estimate for the lattice parameter of the material, *a*, in the position being interrogated. In contrast, ILL in France and ANSTO in Australia are both reactor sources, where strain measurements are carried out using neutrons of a single wavelength. At such facilities, Bragg's law of diffraction is applied to measure the spacing, *d*, between specific {*hkl*} crystallographic planes, and this spacing is represented by d_{hkl}. Such measurements can be more vulnerable to texture within the material and to intergranular strains. However, errors can be mitigated to some degree by selecting a wavelength for the neutrons that generates measurements from a crystallographic plane that is known to be relatively insensitive to these effects. In this work, the {211} crystal plane was employed for all measurements made at reactor sources on ferritic steels.

Once values for either the lattice parameter, *a*, or the inter-planar spacing, d_{211}, were obtained at a particular location (x, y) within the measurement plane (Fig. 1), the strain in either the longitudinal (L), transverse (T) or normal (N) direction, $\varepsilon_{L(x,y)}$, $\varepsilon_{T(x,y)}$ or $\varepsilon_{N(x,y)}$ was calculated using an expression of the following form:

$$\varepsilon_{L(x,y)} = \frac{a_{L(x,y)} - a_{0(x,y)}}{a_{0(x,y)}} \quad (1)$$

In eq. (1), the parameter $a_{0(x,y)}$ is the stress-free lattice parameter at the position (x, y) of interest. The method that was employed for determining the stress-free lattice parameter will be described in a later section. In all cases in this work, the longitudinal direction corresponds to the *z*-direction as defined in Figure 1, while the transverse direction corresponds to the *x*-direction, and the normal direction corresponds to the *y*-direction. In cases where a reactor source was used, the parameter $a_{L(x,\,y)}$ in eq. (1) must be replaced by $d_{L\{211\},(x,y)}$, and the parameter $a_{0(x,\,y)}$ must be replaced by $d_{0\{211\},(x,y)}$.

Having determined the values for strain in the three mutually orthogonal (L, T, N) directions, the stresses acting in each of these directions $\sigma_{L(x,y)}$, $\sigma_{T(x,y)}$ and $\sigma_{N(x,y)}$ were calculated using a generalised expression based on Hooke's law, which had the following form:

$$\sigma_{L(x,y)} = \frac{E}{1+\nu}\left[\varepsilon_{L(x,y)} + \frac{\nu}{1-2\nu}\left(\varepsilon_{L(x,y)} + \varepsilon_{T(x,y)} + \varepsilon_{N(x,y)}\right)\right] \qquad (2)$$

In cases where the data were measured at ISIS, bulk values for E and *v* (209 GPa and 0.3) were employed in the determination of stresses. However, for cases involving data that were obtained from a reactor source, plane-specific values (216 GPa and 0.3) were used, following Daymond and Priesmeyer [21].

In all cases, a gauge volume for the longitudinal strain measurements of 3 mm × 3 mm × 3 mm was employed, while for the measurement of strains in the transverse and normal directions the gauge volume had the dimensions of 3 mm × 3 mm × 10 mm, with the gauge volume being elongated in the welding (z) direction. It is reasonable to elongate the gauge volume in this way because, under steady-state welding conditions, the gradients in strain (and hence in stress) should, in principle, be zero in this direction. Elongation of the gauge volume in this manner also leads to a reduction in measurement times, and it therefore provides for more efficient use of the beam time that is available.

2.6.1 Measurement Array

Figure 3 shows the arrangement of measurement points within the measurement plane, the location of which is shown in Figure 1. All neutron diffraction measurements were carried out within the measurement plane. It can be seen that the density of measurement points was high in the vicinity of the weld centreline, where both the stresses and the stress gradients were expected to be high. The density of measurement points decreased with increasing distance from the weld centerline, where both the magnitude of the stresses and the stress gradients were expected to decrease. Values for either *a*, or d_{211}, were measured at all points (both open and solid) that are shown in Figure 3, making 53 measurement locations in total.

2.6.2 Stress-Free Lattice Parameter

In order to determine strain, and hence stress, in a weld test piece it is necessary to compare the measured lattice spacing (or interplanar spacing), at a particular location, with the lattice spacing (or interplanar spacing) that is measured in nominally identical material (in terms of chemical composition, microstructure and degree of work hardening), which is also free of macroscopic stress. In order to achieve this, a comb-shaped specimen was extracted from the corresponding location in a nominally identical weld, for each of the weld types interrogated in this study. Electric-discharge machining (EDM) was used to extract the comb-shaped specimens in order to avoid work hardening of the material. An outline of the comb specimens is shown in Figure 3. By making cuts in the material, the majority of the macroscopic stresses that were present in the material would have relaxed, since the material would no longer have been constrained by surrounding material. In this way, the material would have approached a (macroscopic) stress-free state.

Values for the stress-free lattice parameter, a_0, or the stress-free interplanar spacing, $d_{0\{211\}}$, were measured at the solid points in Figure 3. It is important to make a significant number of measurements in the vicinity of the weld [22], since there will be significant variations in the microstructure in this region. The value of a_0 (or $d_{0\{211\}}$) should have been relatively uniform across the unaffected parent material, so fewer measurements were made in the far field. In this work, an average value was used for far-field values of a_0 (or $d_{0\{211\}}$) in each specimen, in order to obtain the most reliable estimate for this parameter far from the weld. Values were judged to be in the far field if they were 10 mm or more from the fusion boundary on either side of the specimen, after referring to a weld macrograph.

2.7 Contour Method Measurements

Contour method residual stress measurements were made in both the AW and PWHT conditions. In all cases the necessary EDM cuts in the 30 mm thick plates were made on a transverse plane at the weld mid-length, thereby recovering the longitudinal stresses on this plane. In this work, the contour method measurements were carried out in the following four steps:

- EDM cutting;
- Measuring out-of-plane deformations (i.e. the contour) on the EDM-cut surface;

- Data processing (averaging and fitting (smoothing) of the surface); and
- Carrying out an elastic finite element analysis to calculate stresses.

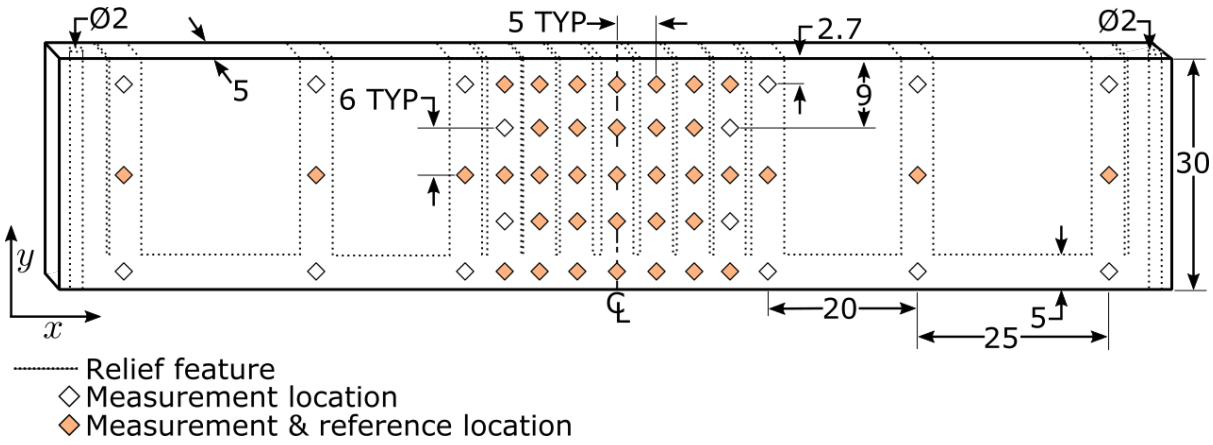

Figure 3: Spatial distribution of measurements within the measurement plane (see Fig. 1) for neutron diffraction experiments. Strains were measured at both open and solid points, while values for a_0 or $d_{0\{211\}}$ were measured only at solid points. An outline of the comb specimens is also shown, along with the positions of the pilot holes for contour method measurements.

Wire electric discharge machining (EDM) was selected as a technique that would fulfil the requirements [23] for achieving a straight cut and minimising the stresses that are generated during the cutting operation. Cutting was performed in a GF Agie Charmiles FI 440 ccS wire-EDM machine, with cutting parameters that were optimised for SA508 Grade 3 Class 1 steel through a number of trials. The cuts were made between pre-drilled pilot holes, positioned 12 millimetres from the edges of the plate in each case, in order to minimize plasticity during the cutting process, since plastic deformation during cutting is a major source of systematic errors in contour method measurements [24]. The locations for the pilot holes, which had a diameter of 2 mm, are shown in Figure 3.

Figure 4 shows the clamping arrangement for the specimens during EDM cutting. The arrangement was designed to prevent movement of the sample while avoiding the undesirable forces that conventional clamping techniques would normally introduce. Adjustable thrust pads were brought into contact with copper sheets, which were placed on the top and bottom surfaces of the sample, by adjusting a set of screws that passed through

each of the restraining bars. Restraining bars and adjustable thrust pads were located on both sides of the sample. In this way, it was possible to ensure good contact, but also to avoid forcing a distorted sample down on to a flat surface: an approach that would have led to the introduction of bending stresses to the test piece. A number of thrust pads were located close to the cutting plane, which has been identified as good practice for the mitigation of plastic flow as cutting progresses [25, 26]. Any effects associated with the clamping arrangement are likely to be most significant for the transverse residual stresses, and in this work the contour method has been used to measure the longitudinal residual stress distributions. As such, the authors were of the view that the benefits associated with the minimisation of plasticity errors through clamping were likely to be more significant than the potential for introducing errors.

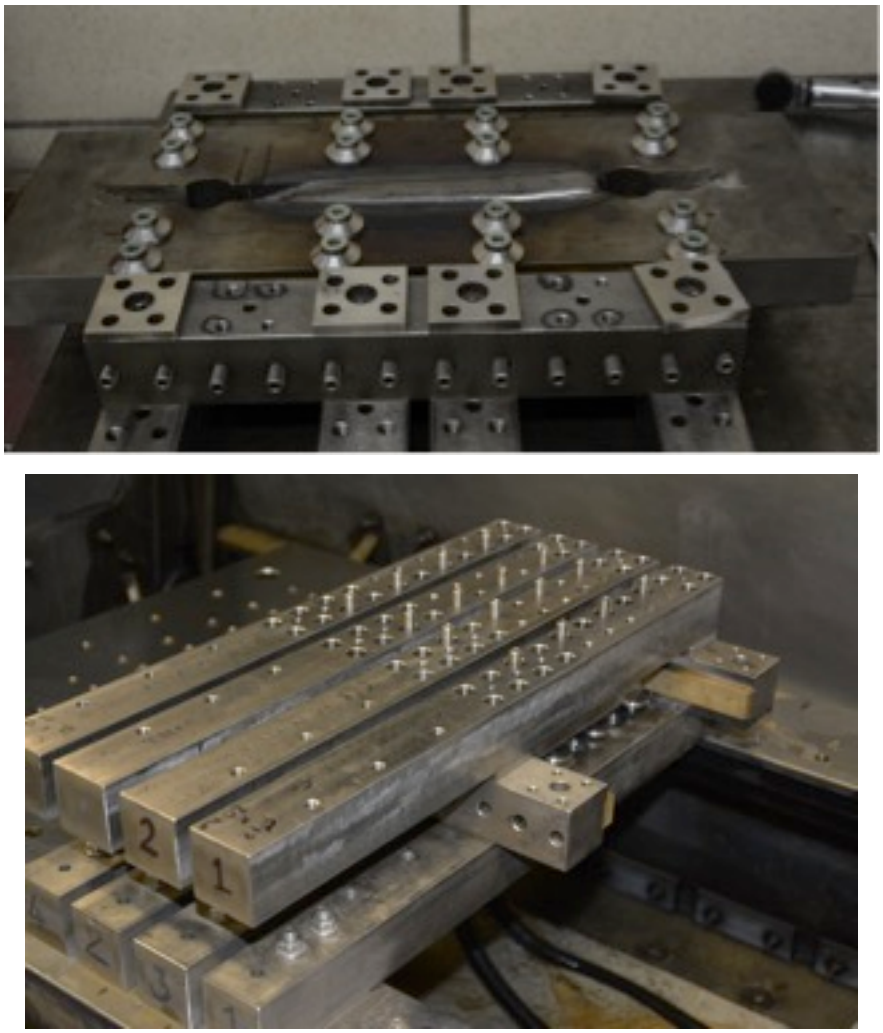

Figure 4: Clamping arrangement for contour method (EDM) cutting process. An NG-SAW test piece can be seen prior to (top) and after (bottom) fixing of the restraining bars.

For the surface profilometry, a Nanofocus laser scanner was used, with the distance between measurement points set to 30 microns. Processing of the surface profile data is a multi-stage process [27] and several issues need to be considered [28]. Data are initially cleaned and the surface outlines are captured. Averaging of the two cut surface profiles is required, to eliminate errors associated with cutting and localised plasticity. A bi-variate cubic spline is then fitted to the averaged surface (a smoothing operation), based on a least-squares fitting procedure. The points where the 3rd order polynomials of the spline are joined are called the 'knots', with the knot-spacing being a parameter that can be adjusted according to the anticipated level of detail in the data [29]. In this work, trials were undertaken to identify the best compromise between removing noise and losing information. On this basis, a knot-spacing of 0.5 mm was selected.

The model for the finite element analysis (FEA) was created in ABAQUS, using quadratic (C3D20) elements. The processed surface profile data were imported to the model and applied as displacement boundary conditions. Additional boundary conditions were applied to prevent rigid body motion. An elastic analysis was performed, since the primary assumption [23] underpinning the contour method is that all out-of-plane deformations result from the elastic relaxation of stress. While the method can be employed with excellent results, one must always be alert to the potential for plasticity-induced errors when interpreting the results.

All except one of the contour maps and line plots for residual stress that are presented in this work were derived using the methodology and parameters that are described above. The only case that required different treatment was the RPEB weld, for which the measured data had to be treated differently in order to capture the M-shaped residual stress distribution in the vicinity of the weld [17]. Owing to the steep gradients in stress, this feature could only be captured using data that were subject to less smoothing, at the expense of retaining a greater level of noise in the fitted stress profile.

3 Distortion, Metallography and Hardness Results

3.1 Distortion Measurements

An example of the type of data that can be obtained from the three-dimensional laser scanning system is given in Figure 5, and the measured butterfly distortion angles are listed in Table 3. It can be seen that some distortion was measured in each case, with the RPEB weld leading to the lowest level of distortion. The NGLW process also led to a very low level of distortion, while a greater degree of distortion was observed for the arc welding processes. The NG-GTAW test piece was associated with the highest level of distortion, presumably owing to the fact that a high number (25) of weld passes was employed using a relatively high weld heat input. Overall though, the levels of distortion are not excessive when consideration is given to the sizes of the test pieces that were employed and the fact that the level of restraint that was applied during welding was low.

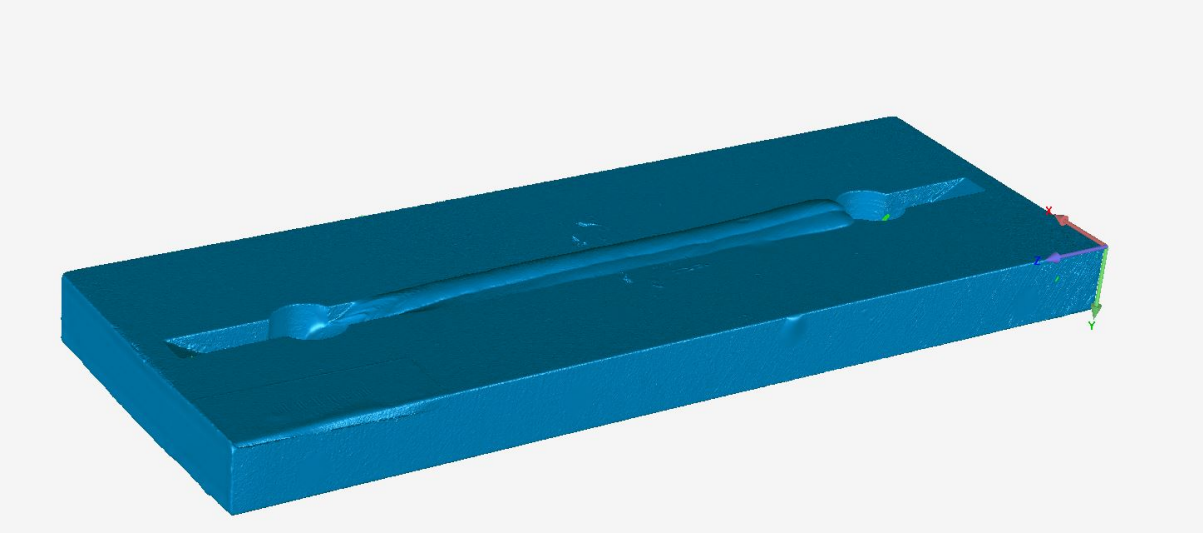

Figure 5: Three dimensional surface profile of the NG-SAW test piece as obtained by laser scanning after the completion of welding.

Table 3: Butterfly distortion angles for test pieces manufactured with each welding process.

Butterfly angle (degrees)			
NG-SAW	**NG-GTAW**	**NGLW**	**RPEB**
1.86	2.6	0.73	0.27

3.2 Weld Macrographs

Macrographs for each type of weld are shown in Figure 6. It can be seen that each welding process generated sound welds. It is worth noting the differences in the weld width for each of these processes. The narrowest fusion zone was produced by RPEB welding (~ 4 mm). However, the fusion zone for the NGLW process (~ 10 mm) was also considerably narrower than those for each of the arc welding processes. Even though the total volume of weld metal that was deposited using the NGLW process was significantly lower than for the arc welding processes, it is worth noting that the deposition rate with NGLW is significantly lower than for NG-SAW, for example. As such, from a productivity standpoint, the benefit of depositing less metal per unit length of weld with NGLW is to a significant extent offset by its lower deposition rate.

3.3 Hardness maps

Hardness maps are presented in Figure 7 for each type of weld, and for test pieces in both the AW and PWHT conditions. It can be seen that both arc welding processes result in some level of pass-to-pass tempering, so that hardness values are not extremely high in the AW condition, except for in the vicinity of the last weld pass. Some degree of pass-to-pass tempering also occurs in the NGLW test piece, but to a much lesser extent, while none occurs in the single pass RPEB weld. PWHT is effective in all cases, bringing hardness values to < ~ 300 HV. Higher hardness values persist in the RPEB weld, presumably due to the lack of pass-to-pass tempering, and also due to the higher carbon content that would have been present in an autogenous weld.

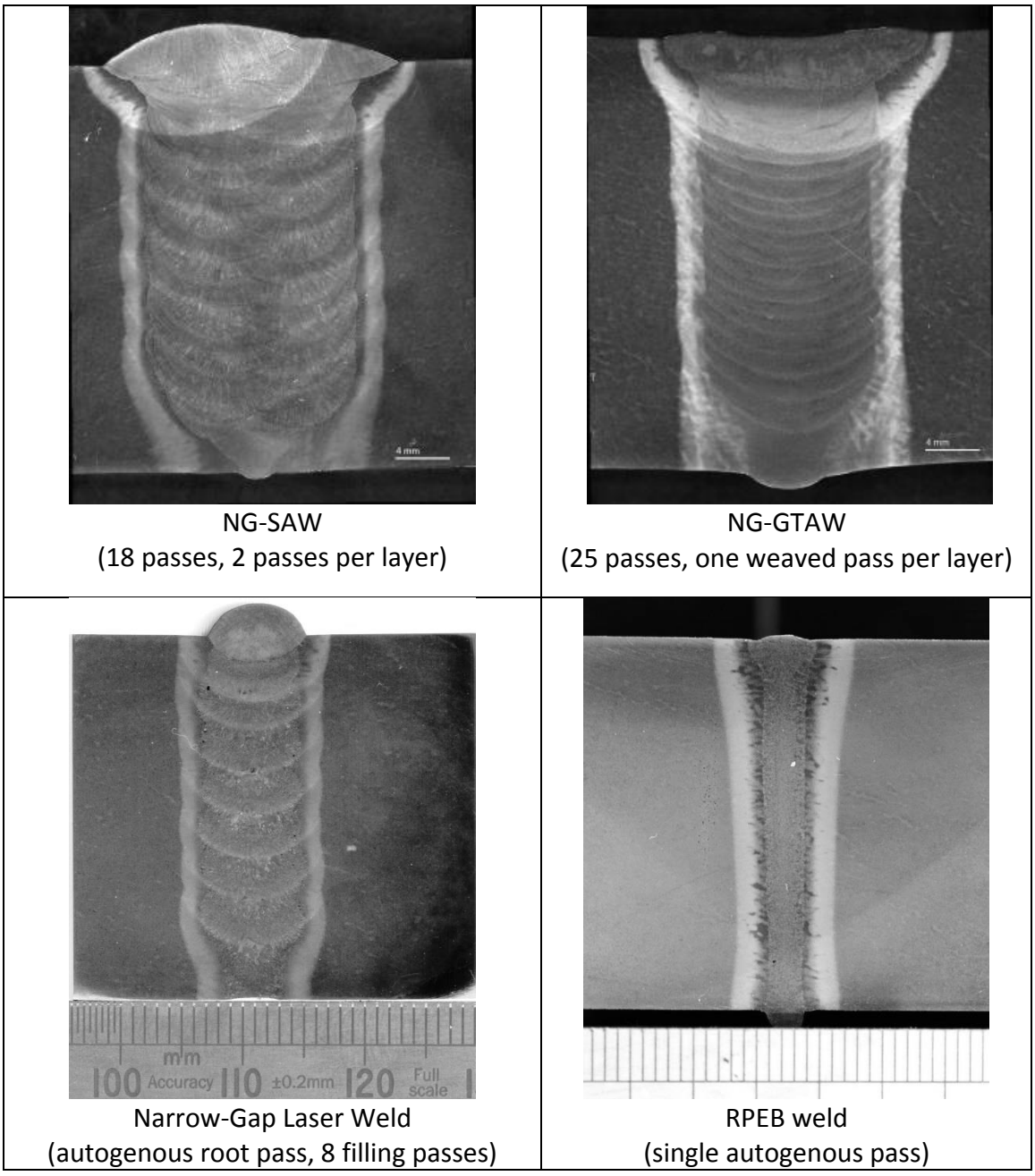

NG-SAW
(18 passes, 2 passes per layer)

NG-GTAW
(25 passes, one weaved pass per layer)

Narrow-Gap Laser Weld
(autogenous root pass, 8 filling passes)

RPEB weld
(single autogenous pass)

Figure 6: Macrographs for each type of weld: NG-SAW (top left), NG-GTAW (top right), NGLW (bottom left) and RPEB weld (bottom right).

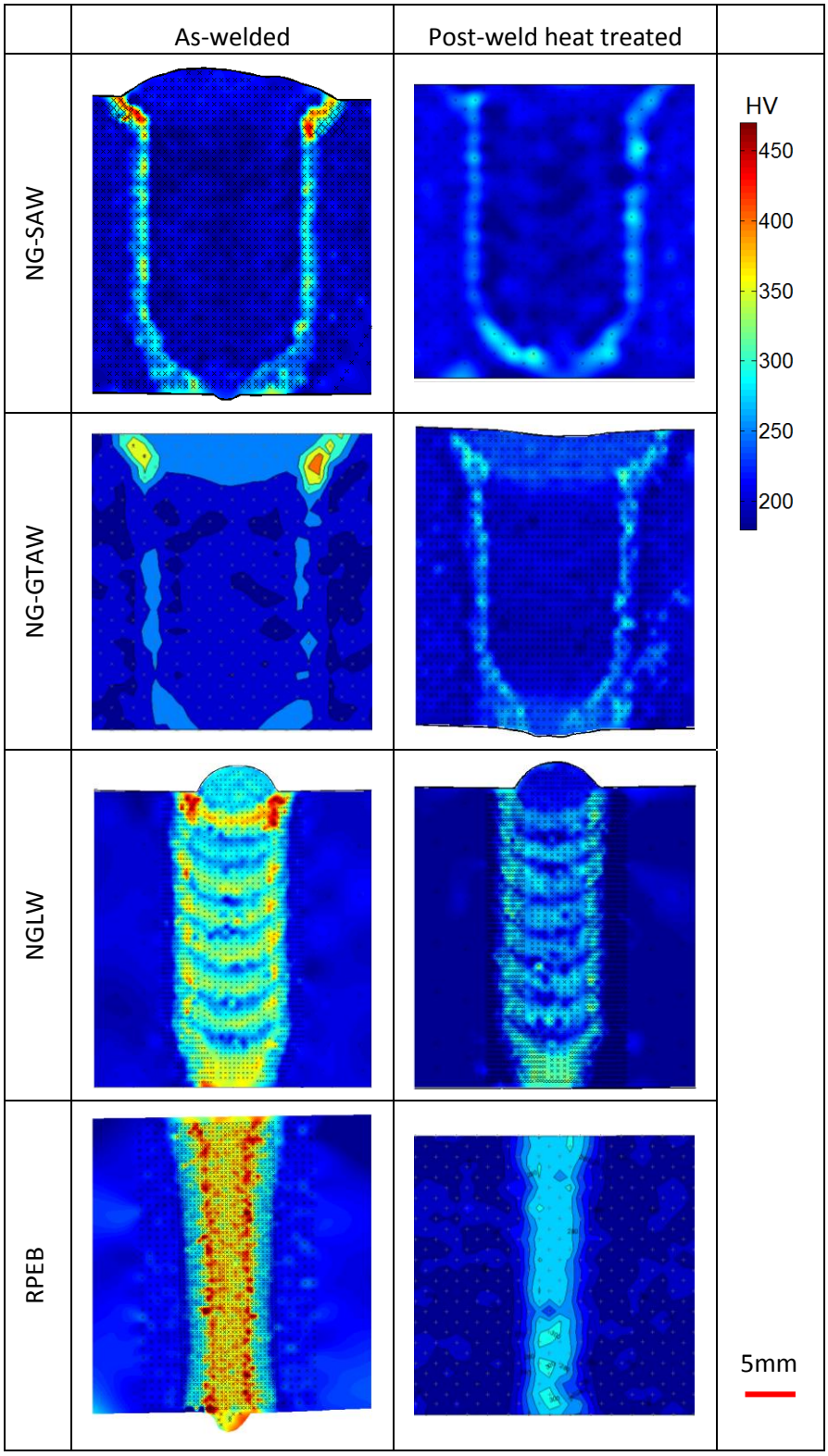

Figure 7: Hardness maps for the NG-SAW (top), NG-GTAW (second from top), NGLW (third from top) and RPEB welds in the AW (left) and PWHT (right) conditions.

4 Residual Stress Measurements - Results and Discussion

4.1 Measurements in As-Welded Condition

The longitudinal residual stresses that were measured for each of the welding processes are presented in Figure 8. The results that were obtained using neutron diffraction and using the contour method are presented side by side so that the level of agreement between each of the techniques can be assessed. It can be seen that the agreement between the techniques is generally very good.

The residual stress distribution that differs most significantly from the others is that for the RPEB process. In particular, a region of low-magnitude or mildly compressive residual stress can be seen to exist at the weld centreline, while the regions of peak tensile residual stresses reside a few millimetres to either side of the weld centreline. This type of residual stress distribution is known to result from the effects of the solid-state phase transformations that take place within the steel during welding [10, 16, 17], and it is also a consequence of the RPEB process being a single-pass process. In all of the other test pieces, subsequent weld passes will have resulted in reheating of the regions that were subject to solid-state phase transformations, leading to regions within the fusion zone, excluding the final capping pass, which sustain high levels of tensile residual stresses.

Among the multipass welding processes, the tensile residual stresses in the NG-SAW and NGLW test pieces appear to be consistently high throughout the fusion zone and HAZ. While this observation is not yet fully understood, it may be related to the steep temperature gradients that would have been introduced by each of these processes. Although SAW is not normally associated with steep temperature gradients, the welding speed for NG-SAW in this work was substantially higher than it was for NG-GTAW, and the heat source power (voltage × current) was low for what might be considered typical for NG-SAW, being slightly lower than (but in the order of) the beam power that was used in the NGLW. (These choices for NG-SAW were related to the size of the test pieces being welded, and the corresponding choice for the diameter of the filler wire.) One would therefore expect the temperature gradients in the NG-SAW weld to be at least as steep as they would have been in the NGLW sample. When the temperature gradients are particularly steep, the extent of the surrounding material that is subjected to significant re-heating will remain small, and this

may result in highly tensile residual stresses persisting within previously deposited weld metal.

It is clear that, for the NG-GTAW weld, there is a region that is sustaining high levels of tensile residual stress, but that this region does not span the entire fusion zone. For this process in particular, this is understandable, owing to the very low welding speed that was employed. By travelling slowly, the temperature gradients will have been relatively modest (for a fusion welding process) and this will have resulted in substantial reheating of previously deposited weld metal. This, in turn, may have contributed to the alleviation and/or redistribution of tensile residual stresses in previously deposited weld metal.

In all cases, regions of peak tensile residual stress in the order of the yield stress exist in the vicinity of the weld region, and these stresses gradually decay before becoming compressive at greater distances from the weld centreline. If the plates were infinitely wide, the stresses would be expected to decay towards zero in the far field (assuming that the parent material is relatively free of stress). However, in this programme of work, it appears that the plates were not always sufficiently wide for this to be the case. This is not problematic from the standpoint of understanding the effects of each process, as the data that have been obtained will ultimately serve to validate numerical modelling methodologies, which can be used retrospectively to assess the effects that finite plate dimensions might have had on the development of stresses.

A final observation would be that the extent and the detailed features of the distribution of peak tensile residual stresses do vary according to the welding process, the welding parameters that were employed, and the number of passes that was used to make the weld. There is some variability in the details of the residual stress distributions in the vicinity of the fusion zone, particularly in the case of the neutron diffraction measurements. This is not unexpected, as it is known that neutron diffraction measurements are often problematic in the weld metal region [30], as it can be difficult to obtain reliable measurements for the stress-free lattice parameter. Overall though, the AW tensile residual stress distributions present a relatively consistent picture. It would appear that the extent to which previously deposited material is reheated by subsequent weld passes is significant in determining the extent to which residual stresses in previously deposited weld metal may be alleviated or redistributed by subsequent welding thermal cycles.

4.2 Measurements in PWHT Condition

The longitudinal residual stresses that were measured in the PWHT condition for each of the welding processes are presented in Figure 9. It can be seen that the PWHT operation has generally been effective in relieving residual stresses, as the stresses are greatly reduced when compared to the corresponding plots for the samples in the AW condition. However, it should be noted that the residual stresses were not removed altogether and that, in some cases, residual stresses in excess of 100 MPa persist. From a structural integrity standpoint, this may not be of concern at the start of life when ferritic steels components exhibit upper shelf toughness. However, it may become significant as components age within a reactor, particularly if neutron irradiation leads to shifts in the ductile-to-brittle transition temperature [15], thereby creating a situation in which components have toughness values that reside on the shoulder of the transition curve.

While the results for the PWHT condition generally provide a consistent picture, the results for the NG-GTAW weld, as obtained by neutron diffraction, appear to be anomalous. The authors believe this is due to problems associated with obtaining reliable measurements for the stress-free lattice parameter in this test piece.

4.3 Measurements for Transverse Residual Stresses

The measurement of transverse residual stresses (Figure 10) in welded components by neutron diffraction can be unreliable for reasons that are not fully clear [30]. It is possible that sources of uncertainty arise in part as a consequence of the difficulties associated in measuring the stress-free lattice parameter in weld metal. The patterns that were observed in the transverse stresses that were measured in this work also appeared to be somewhat erratic, which suggests that some caution should be applied in interpreting the results.

One of the “sanity checks” that can normally be carried out on the transverse residual stresses, assuming that the weld traversed the full length of the specimen and that the heat source was always centred on the weld centerline, is that the transverse stresses should not introduce a net bending moment across the thickness of the specimen. In this study, however, the specimen geometry was such that ligaments of material remained intact at either end of the specimen for each of the multipass welds. On this basis, the form of the

transverse residual stress distribution in the NG-GTAW specimen, for example, cannot be assumed to be incorrect at first glance.

The transverse stresses in the electron beam weld are likely to be low, in reality, across the entire measurement plane. This assertion is based on the weld being a single-pass weld in which the extent of the fusion zone and HAZ is fairly consistent throughout the thickness of the plate. The weld was also made along the full length of the plate, without any external restraint. There are, therefore, no obvious contributing factors to the generation of bending stresses that might act on the plane of the weld centerline. In can be seen, however, that there are some significant spikes in compressive stress located in the vicinity of the fusion zone. These are likely to be artifacts associated with variability in the values that were measured for the stress-free lattice parameter, and they reflect the degree of caution that must be applied when examining measurements from a single technique in isolation. In contrast, the multipass welds were all subject to factors that would lead to the generation of bending stresses on the plane of the weld centerline. The most important of these factors is the fact that the welds involved a number of passes, which were all deposited from the same side of the plate.

There are some consistencies in the patterns observed in the NG-SAW and NGLW samples, with tension at the top of the weld, compression at the mid-thickness position, returning to tension at the back surface, with maximum tensile stresses being between 200 and 300 MPa in each case. Although the distribution of the transverse residual stresses in the NG-GTAW sample is somewhat different, maximum tensile stresses in the order of 300 MPa were also observed. Thus, the maximum transverse residual stresses were observed to be in the order of 50% of the peak values in longitudinal residual stresses.

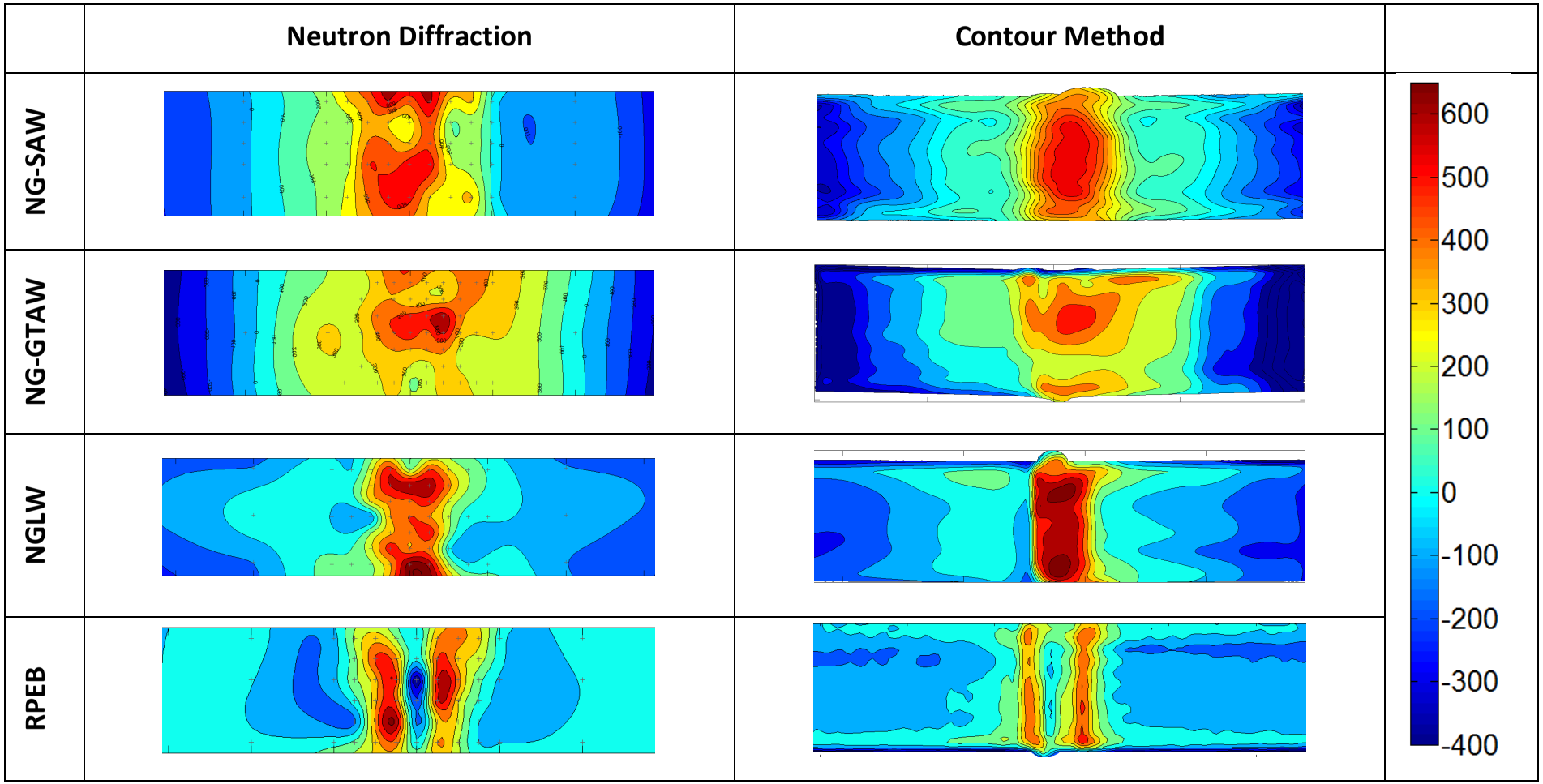

Figure 8: Longitudinal residual stresses (MPa) in the AW condition for each welding process, as measured using neutron diffraction and the contour method.

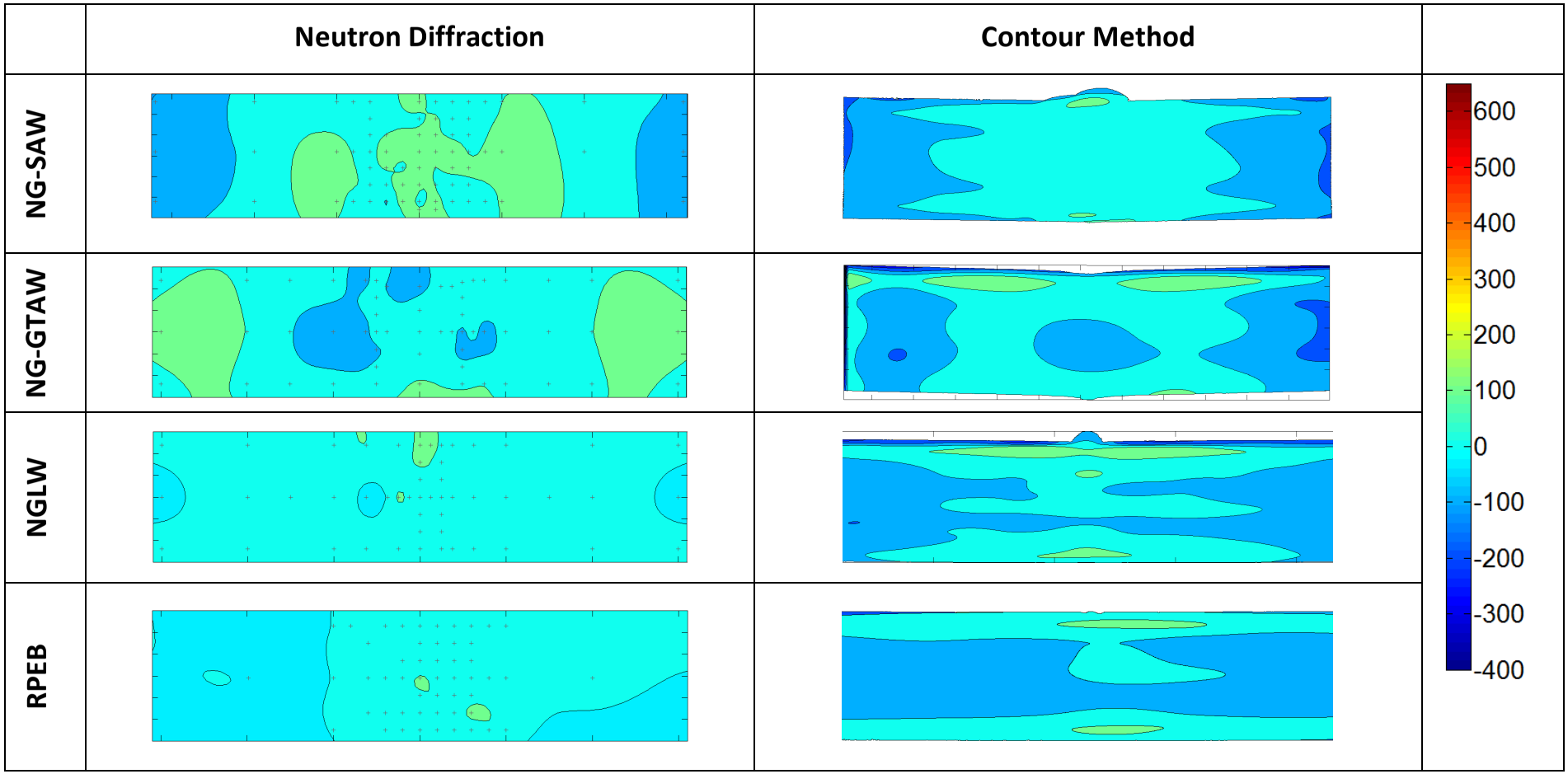

Figure 9: Longitudinal residual stresses (MPa) in the PWHT condition for each welding process, as measured using neutron diffraction and the contour method.

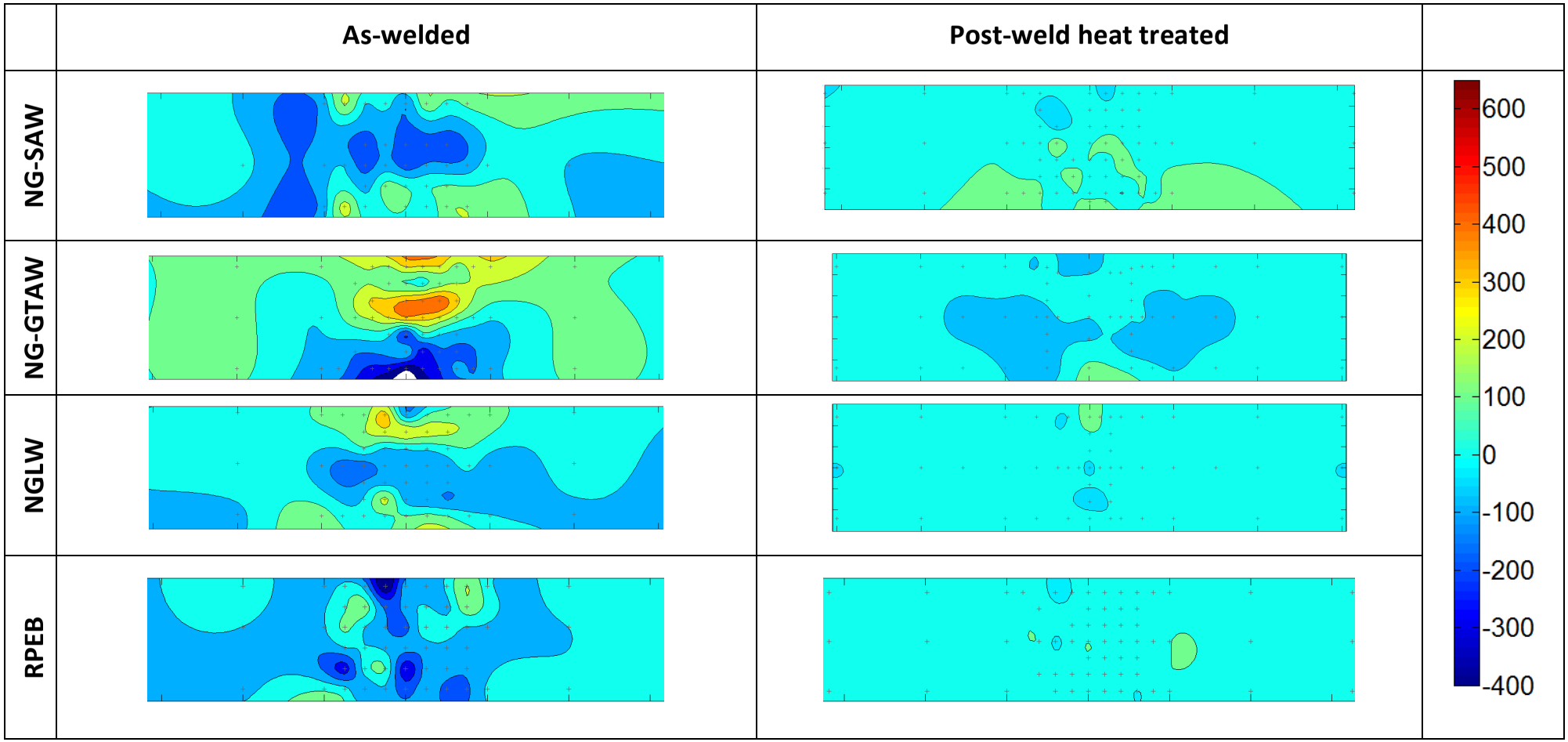

Figure 10: Transverse residual stresses (MPa) as measured by neutron diffraction for each welding process, in the AW condition (left) and after PWHT (right).

4.4 Comparison of Stresses Measured with Each Technique

The longitudinal residual stresses that were measured with neutron diffraction and the contour method at the mid-thickness position are compared in Figure 11 for each welding process. It can be seen that, in general, excellent agreement is achieved between the measurement techniques, which provides broader confidence in the longitudinal stresses that were measured in this work. Peak tensile residual stresses in the order of 600 MPa were measured for each welding process, which is consistent with previously published measurements on SA508 Grade 3, Class 1 steel [9] and corresponds approximately to the UTS for the steel. It is worth noting that residual stresses in the order of the UTS are feasible when multi-axial residual stresses are present. The very high value of tensile stress that was obtained by neutron diffraction, near the weld centreline in the NGLW sample, is almost certainly anomalous, potentially resulting from a spurious value for the stress-free lattice parameter.

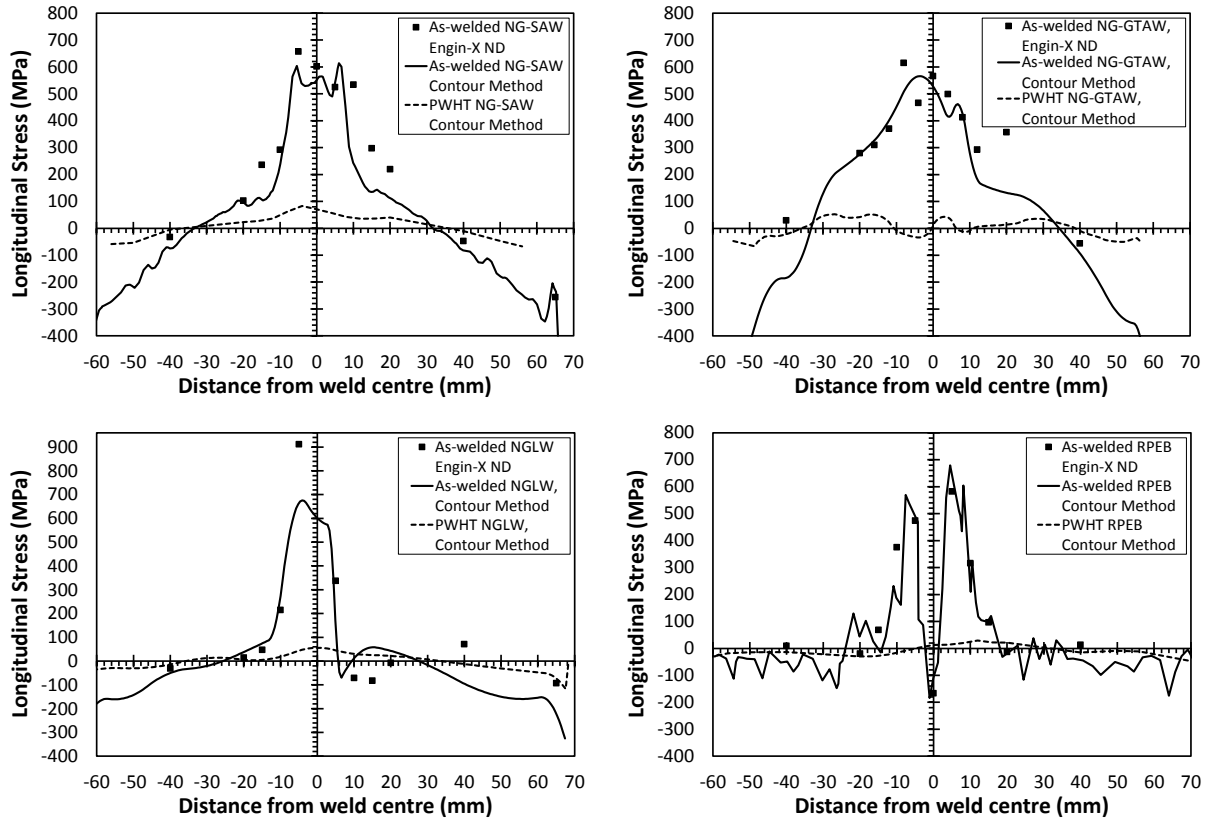

Figure 11: Line plots showing the longitudinal residual stress distributions measured at the mid-thickness position for each welding process before and after PWHT.

The characteristic “M-shaped” residual stress measurement profile was obtained with both measurement techniques in the RPEB weld, which is reassuring. Another interesting observation is that the width of the region sustaining highly tensile residual stresses can also be discerned for each of the welding processes in Figure 11. Among the multipass welding processes, NGLW has the narrowest tensile region, followed by NG-SAW, with NG-GTAW having the widest tensile region. In all cases, PWHT has been effective in reducing the levels of residual stress, with values at the mid-thickness position generally being reduced to 100 MPa or less.

5 Summary

In the present work, the manufacture, measurement and analysis of residual stresses has been described in 30 mm thick specimens, for four welding processes that were applied to SA508 Grade 3 Class 1 steel. Some clear trends have emerged and it is possible to draw definitive conclusions. These conclusions include the following:

- Good overall agreement was achieved between the longitudinal residual stresses that were measured using the contour method and neutron diffraction. All welding processes produced peak tensile residual stresses in the order of the UTS for SA508 Grade 3 Class 1 steel. The peak tensile residual stresses reside in the vicinity of the weld region in all cases, and decrease in magnitude with increasing distance from the weld centerline, until they become compressive in the far field.
- The distribution of the peak tensile residual stresses varied according to the welding process. RPEB welding produced a longitudinal residual stress distribution that displayed the characteristic M-shape, being of a low magnitude on the weld centerline, and having regions of peak tensile residual stress immediately outside the heat affected zone. This distribution is known to result from the solid-state phase transformations that take place in SA508 Grade 3 Class 1 steel during welding, in combination with the fact that only a single welding thermal cycle was employed. The distributions for the other welding processes are complicated to a varying degree, owing to the fact that multiple weld passes were employed. The tensile residual stresses were high throughout the entire weld thickness for the NGLW, as

well as for the NG-SAW test piece. This may be related to the welding parameters that were employed in each case, which will have led to particularly steep temperature gradients during welding. In contrast, the NG-GTAW specimen did not sustain peak levels of tensile residual stress throughout the entire thickness, which may be related to the slow welding speed that was employed, in combination with a weave welding configuration.

- Among the multipass processes, the width of the region of peak longitudinal tensile residual stresses was maximum for the NG-GTAW weld, followed by the NG-SAW and the NGLW test pieces. The distribution for the RPEB weld is not directly comparable since the stresses on the weld centerline are close to zero, if not slightly compressive, owing to the effects of solid-state phase transformations. However, the outer boundaries of the regions sustaining peak tensile residual stresses reside at a similar distance from the weld centerline as for the NG-SAW test piece.
- The interpretation of the measured transverse residual stresses was more challenging. In the case of the multipass welds, the peak tensile stresses appear to be (~50%) lower in magnitude than the peak longitudinal residual stresses. There are some unusual and localised spikes in the measured transverse residual stresses which may be artifacts associated with variability in the measured values for the stress-free lattice parameter.
- Post-weld heat treatment (PWHT) was effective in reducing the levels of residual stress that were present in all of the welded test pieces. However, values of residual stress in the order of 100 MPa were measured in specimens after PWHT. While residual stresses may not be of concern when a steel is clearly exhibiting upper shelf toughness, these levels may be of concern in aging vessels that have experienced a shift in the ductile-to-brittle transition temperature.
- The peak tensile residual stresses in the RPEB weld were comparable to those for the other processes so, from this standpoint, the RPEB process may not offer advantages in terms of the susceptibility of a welded joint to brittle fracture. However, this is unlikely to present an obstacle to the adoption of RPEB welding, since a major advantage of the RPEB process is that it reduces typical welding times by an order of magnitude when compared to current practice.

6 Further Work

In carrying out the research that has been described in this article, some important areas for further work were identified:

- While this investigation has focused on the welding of ferritic steels, the RPEB process can also be applied to austenitic stainless steels and other materials in which the final state of stress will not be affected by solid-state phase transformations. It would clearly be informative to carry out a similar cross-process comparison on a material that falls within this category.
- Further questions will need to be answered before the RPEB welding process can be applied to safety-critical components with confidence. For example, RPEB welding is autogenous, which means that the weld metal can be expected to have the same nominal chemical composition as that of the parent material. In the case of ferritic steels this might mean that RPEB weld metal will have a higher carbon concentration than arc-deposited weld metal. Any potential implications for weld toughness will need to be explored. Such work should also address the potential influence of the different fusion zone and HAZ geometries on the potential for through-wall crack propagation.
- A comprehensive cross-process comparison of the type described in this work should also involve the testing of mechanical properties such as strength and toughness. The authors are currently addressing this issue for welds made with the same steel that was used in this study, but at the greater thickness of 130 mm. This work will be reported in the near future.

7 Acknowledgements

The authors gratefully acknowledge financial support provided by the Engineering and Physical Sciences Research Council (EPSRC) through the NNUMAN programme grant in nuclear manufacturing (Grant number: EP/J021172/1), and the Manufacturing Fellowship EP/L015013/1. The authors are also grateful for the provision of beam time on the Engin-X instrument at ISIS, on the SALSA beam line at ILL, and on the Kowari beam line at ANSTO. The authors would like to thank Drs. S. Kabra, A. Paradowska and M. Reid for assistance with the neutron diffraction measurements, and Dr. R. Scott at the Advanced Manufacturing

Research Centre (AMRC) in Rotherham, U.K., for access to the laser scanning system. The authors are also grateful for technical assistance from Dr. Joanna Walsh, Mr. Ian Winstanley and Mr. Paul English, and for support from Ms. J. Grant.

8 References

[1] A. S. Sanderson, C. S. Punshon and J. D. Russell: “Advanced welding processes for fusion reactor fabrication”, Fusion Engineering and Design, **49-50**, pp. 77-87, 2000.

[2] K. R. Ayres, P. R. Hurrell, C. M. Gill, K. Bridger, L. D. Burling, C. S. Punshon, Liwu Wei and N. Bagshaw: “Development of Reduced Pressure Electron Beam Welding Process for Thick Section Pressure Vessel Welds”, Paper PVP2010-25957, Proceedings of the ASME 2010 Pressure Vessels and Piping Division Conference, Bellevue, Washington, USA, July 18–22, 2010.

[3] D.P.G. LIDBURY: “The Significance of Residual Stresses in Relation to the Integrity of LWR Pressure Vessels”, *International Journal of Pressure Vessels and Piping*, **17** (4), 197-328, 1984.

[4] D.T. READ: “Measurement of Applied J-Integral Produced by Residual-Stress”, *Engineering Fracture Mechanics*, **32** (1), 147-153, 1989.

[5] D.J HORNBACH and P.S. PREVEY: “The Effect of Prior Cold Work on Tensile Residual Stress Development in Nuclear Weldments”, *Journal of Pressure Vessel Technology - Transactions of the ASME*, **124** (3), 359-365, 2002.

[6] D. RADAJ: “Heat Effects of Welding – Temperature Field, Residual Stress, Distortion”, *Springer-Verlag*, Berlin Heidelberg, pp. 1-18, 1992.

[7] R6: Assessment of the integrity of structures containing defects, Revision 4, EDF Energy, Barnwood, Gloucester, U.K., 2009.

[8] J.A. FRANCIS, H.K.D.H. BHADESHIA and P.J. WITHERS: Review – “Welding Residual Stresses in Ferritic Power-Plant Steels”, *Materials Science and Technology*, **23** (9), 1009-1020, 2007.

[9] D. J. Smith, G. Zheng, P. R. Hurrell, C. M. Gill, B. M. E. Pellereau, K. Ayres, D. Goudar and E. Kingston: “Measured and predicted residual stresses in thick section electron beam welded steels”, International Journal of Pressure Vessels and Piping, **120-121**, 66-79, 2014.

[10] J.A. FRANCIS, M. TURSKI and P.J. WITHERS: “Measured Residual Stress Distributions for Low and High Heat-Input Single Weld Beads Deposited on to SA508 Steel”, *Materials Science and Technology*, **25** (3), 325-334, 2009.

[11] W. GUO, S. DONG, J. A. FRANCIS, W. GUO, L. LI: “Microstructure and Mechanical Characteristics of a Laser Welded Joint in SA508 Nuclear Pressure Vessel Steel”, *Materials Science and Engineering A*, **625**, 65-80, 2015.

[12] A.F. MARK, J.A. FRANCIS, M. TURSKI, H. DAI, P.R. HURRELL, S.K. BATE, J.R. KORNMEIER and P.J. WITHERS: “Evolution of Local Material Properties and Residual Stress due to Thermal Cycling in a Multipass SA508 Steel Weld”, *Acta Materialia*, **60**, 3268-3278, 2012.

[13] J. C. Feng, D. W. Rathod, M. J. Roy, J. A. Francis, W. Guo, N. M. Irvine, A. N. Vasileiou, Y. L. Sun, M. C. Smith and L. Li: “An Evaluation of Multipass Narrow Gap Laser Welding as a Candidate Process for the Manufacture of Nuclear Pressure Vessels”, International Journal of Pressure Vessels and Piping, **157**, 43-50, 2017.

[14] B. Jeyaganesh, M. D. Callaghan, J. A. Francis, P. D. English, A. Vasileiou, M. J. Roy, W. Guo, N. M. Irvine, M. C. Smith, L. Li and A. H. Sherry: “Overview of Welding Research under the New Nuclear Manufacturing (NNUMAN) Programme”, Proceedings of the ASME 2014 Pressure Vessels and Piping Conference (PVP2014-29015), Anaheim, California, Vol. 6B, 2014, DOI: 10.1115/PVP2014-29015.

[15] G. R. Odette: “On the Dominant Mechanism of Irradiation Embrittlement of Reactor Pressure Vessels Steels”, Scripta Metallurgica, **17**, 1183-1188, 1983.

[16] J. A. Francis, H. J. Stone, S. Kundu, H. K. D. H. Bhadeshia, R. B. Rogge, P. J. Withers and L. Karlsson: “The Effects of Filler Metal Transformation Temperature on Residual Stresses in a High Strength Steel Weld”, Journal of Pressure Vessel Technology, **131**, 041401-1, 2009.

[17] A. KUNDU, S. KUMAR, K.A. VENKATA, P.J. BOUCHARD, J.A. FRANCIS, A. PARADOWSKA, G.K. DEY and C.E. TRUMAN: “Residual Stresses in P91 Steel Electron Beam Welds”, Science and Technology of Welding and Joining, **18** (1), 70-75, 2013.

[18] P. J. Withers: “Residual Stress and it Role in Failure”, Reports on Progress in Physics”, **70**, 2211-2264, 2007.

[19] G. S. Pawley: “EDINP, The Edinburgh Powder Profile Refinement Program”, Journal of Applied Crystallography, **13**, 630-633, 1980.

[20] A. C. Larson and R. B. Von Dreele: "General Structure Analysis System (GSAS)", Los Alamos National Laboratory Report No. LA-UR-86-748, Los Alamos National Laboratory, Los Alamos, NM, 1986.

[21] M. R. Daymond and H. G. Priesmeyer: “Elastoplastic deformation of ferritic steel and cementite studied by neutron diffraction and self-consistent modelling”, Acta Materialia **50** (6), 1613-1626, 2002.

[22] A.D. KRAWITZ and R. WINHOLTZ: “Use of Position-Dependent Stress-Free Standards for Diffraction Stress Measurements”, *Materials Science and Engineering A*, **185** (1-2), 123-130, 1994.

[23] M. B. PRIME: “Cross-Sectional Mapping of Residual Stresses by Measuring the Surface Contour After a Cut”, *Journal of Engineering Materials and Technology*, **123** (2), 162-168, 2001.

[24] Y. Traoré, F. Hosseinzadeh and P. J. Bouchard: “Plasticity in the contour method of residual stress measurement”, *Adv. Mater. Res*., **996**, 337–342, 2014.

[25] Y. L. SUN, M. J. ROY, A. N. VASILEIOU, M. C. SMITH, J. A. FRANCIS and F. HOSSEINZADEH: “Evaluation of Errors Associated with Cutting-Induced Plasticity in Residual Stress Measurements Using the Contour Method”, Experimental Mechanics, **57**, 719-734, 2017.

[26] Y. JAVADI, J.N. WALSH, A. ELREFAEY, M.J. ROY and J.A. FRANCIS: “Measurement of residual stresses induced by sequential weld buttering and cladding operations involving a 2.25Cr-1Mo substrate material”, *International Journal of Pressure Vessels and Piping*, **154**, 58-74, 2017.

[27] G. JOHNSON: “Residual Stress Measurements Using the Contour Method”, PhD Thesis, *The University of Manchester*, 2008, pp. 243.

[28] F. HOSSEINZADEH, J. KOWAL and P. J. BOUCHARD: Towards good practice guidelines for the contour method of residual stress measurement, *The Journal of Engineering*, DOI: 10.1049/joe.2014.0134.

[29] M. B. PRIME, R. J. SEBRING, J. M. EDWARDS, D. J. HUGHES and P. J. WEBSTER: “Laser Surface-contouring and Spline Data-smoothing for Residual Stress Measurement”, *Experimental Mechanics*, **44** (2), pp. 176–184, 2004.

[30] C. Ohms: PhD Thesis, “Residual Stresses in Thick Bi-metallic Fusion Welds: a Neutron Diffraction Study”, Delft University of Technology, 2013. DOI: 10.4233/uuid:75b3e3a8-399c-4584-ad7b-647a76908415.